Sodium Intercalation Chemistry in Graphite

Journal:	*Energy & Environmental Science*
Manuscript ID:	EE-ART-07-2015-002051.R1
Article Type:	Paper
Date Submitted by the Author:	16-Jul-2015

Complete List of Authors:	Kim, Haegyeom; Seoul National University, Department of Materials Science and Engineering, Research Institute of Advanced Materials (RIAM) Hong, Jihyun; Seoul National University, Department of Materials Science and Engineering, Research Institute of Advanced Materials (RIAM) Yoon, Gabin; Seoul National University, Department of Materials Science and Engineering, Research Institute of Advanced Materials (RIAM); Seoul National University, Center for nanoparticle research, Institute for Basic Science (IBS) Kim, Hyunchul; Sungkyunkwan University, Department of Energy Science Park, Kyu-Young; Seoul National University, Department of Materials Science and Engineering, Research Institute of Advanced Materials (RIAM) Park, Min-Sik; Korea Electronics Technology Institute, Advanced Batteries Research Center Yoon, Won-Sub; Sungkyunkwan University, Department of Energy Science Kang, Kisuk; Seoul National University, Department of Materials Science and Engineering, Research Institute of Advanced Materials (RIAM); Seoul National University, Center for nanoparticle research, Institute for Basic Science (IBS)

SCHOLARONE™
Manuscripts

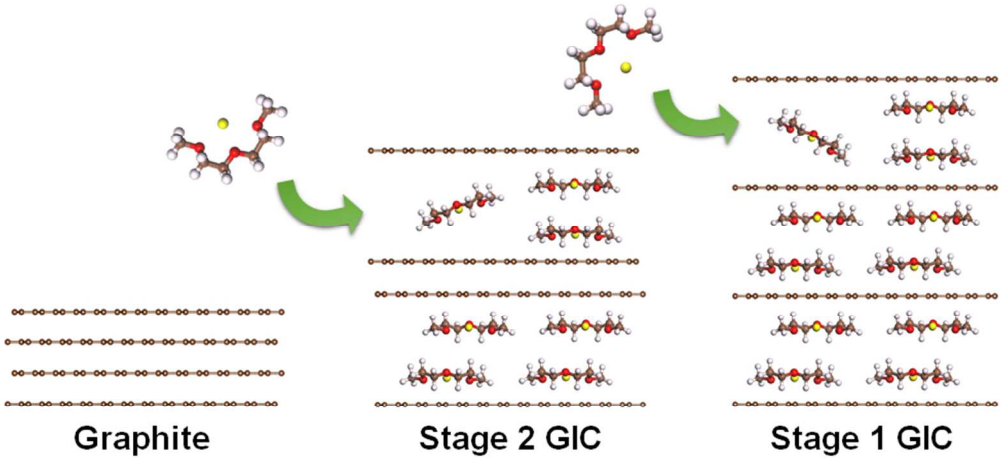

82x44mm (300 x 300 DPI)

Energy & Environmental Science

ARTICLE

Sodium Intercalation Chemistry in Graphite

Haegyeom Kim[a†], Jihyun Hong[a†], Gabin Yoon[a, b†], Hyunchul Kim[c], Kyu-Young Park[a], Min-Sik Park[d], Won-Sub Yoon[c], and Kisuk Kang[a,b*]

Received 00th January 20xx,
Accepted 00th January 20xx

DOI: 10.1039/x0xx00000x

www.rsc.org/

The insertion of guest species in graphite is the key feature utilized in applications ranging from energy storage and liquid purification to the synthesis of graphene. Recently, it was discovered that solvated-Na-ion intercalation can occur in graphite even though the insertion of Na ions alone is thermodynamically impossible; this phenomenon enables graphite to function as a promising anode for Na-ion batteries. In an effort to understand this unusual behavior, we investigate the solvated-Na-ion intercalation mechanism using *in operando* X-ray diffraction analysis, electrochemical titration, real-time optical observation, and density functional theory (DFT) calculations. The ultrafast intercalation is demonstrated in real time using millimeter-sized highly ordered pyrolytic graphite, in which instantaneous insertion of solvated-Na-ions occurs (in less than 2 s). The formation of various stagings with solvated-Na-ions in graphite is observed and precisely quantified for the first time. The atomistic configuration of the solvated-Na-ions in graphite is proposed based on the experimental results and DFT calculations. The correlation between the properties of various solvents and the Na ion co-intercalation further suggests a strategy to tune the electrochemical performance of graphite electrodes in Na rechargeable batteries.

Introduction

Graphite is capable of accommodating a wide range of guest species, including alkali, alkaline-earth, and rare-earth elements; halogens; protons; and Lewis acids between its sp^2-bonded graphene layers.[1] Its versatility also allows more than two different guest species to be intercalated simultaneously in the host structure through a co-intercalation process. Graphite intercalation compounds (GICs), the product of the intercalation, exhibit distinctive physical and chemical properties compared with pristine graphite. Their electronic/magnetic structures and optical and catalytic properties significantly vary with the type of intercalant as well as its concentration.[2] For instance, the electrical conductivity of GICs drastically increases along the *c*-axis (~10^4 times) compared to a/b-axes (~10 times) with a high concentration of ionized guest species.[3-5] The unique structure-property relationship of GICs enables the diverse application of graphite and GICs for energy storage and as catalysts and electrical/thermal conductors.[6-10]

Broader context

This study represents the most comprehensive work on the mechanism of guest ion-solvent co-intercalation in graphite forming ternary GICs, which has been poorly understood because of its complexity and difficulty of quantifying the intercalation of ion-solvent complexes compared with simple intercalation forming binary GICs, such as LiC_6 or KC_8. Our results reveal unexplored co-intercalation mechanisms and the formation of ternary GICs in terms of the stoichiometry, staging structure, and solvated ion configuration. This work also advances our understanding of the correlation between the electrochemical properties and the players in the co-intercalation process; we demonstrate that the intercalation potential of solvated Na-ether complex ions into graphite is tunable by tailoring the length of the solvent species, which determines the thermodynamic stability of the intercalation products by screening the repulsion among charge-carrier ions. Our results will lead to the further advancement of graphite as a practically important potential anode for Na ion batteries and enrich the pool of electrode materials which has been limited to the binary systems of guest ion-host materials to versatile ternary systems of guest ion-solvent-host materials for energy storage.

Graphite has been widely used as a standard anode material in Li-ion batteries, where it forms a series of binary GICs during intercalation and finally reaches the stoichiometry of LiC_6, delivering a high capacity. [11, 12] However, thus far, graphite has not been considered suitable for Na-ion batteries, an alternative system for large-scale energy storage because of the thermodynamic instability of binary Na-intercalated

[a] Department of Materials Science and Engineering, Research Institute of Advanced Materials (RIAM), Seoul National University, Gwanak-ro 599, Gwanak-gu, Seoul 151-742, Republic of Korea
[b] Center for nanoparticle research, Institute for Basic Science (IBS), Seoul National University, Gwanak-ro 599, Gwanak-gu, Seoul 151-742, Republic of Korea
[c] Department of Energy Science, Sungkyunkwan University, Suwon 440-746, Republic of Korea
[d] Advanced Batteries Research Center, Korea Electronics Technology Institute, Seongnam 463-816, Republic of Korea
† These authors are equally contributed to this work.
Electronic Supplementary Information (ESI) available: Experimental and computational details, graphite staging models, ex situ XRD analysis results, and supplementary discussions. See DOI: 10.1039/x0xx00000x

This journal is © The Royal Society of Chemistry 20xx

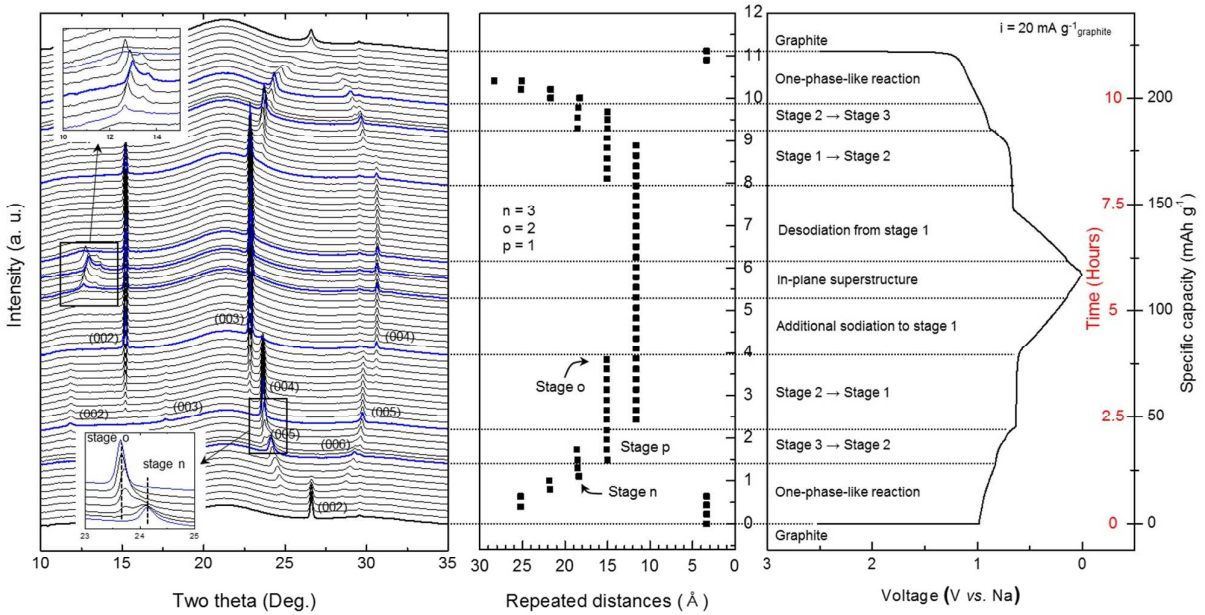

Figure 1. *In operando* synchrotron X-ray diffraction analysis of the structural evolution of the ternary Na-ether-graphite system observed during electrochemical solvated-Na-ion intercalation and deintercalation into/out of graphite in Na | 1M $NaPF_6$ in a DEGDME | graphite cell.

GICs.[13, 14] As a recent breakthrough, Jache *et al.* and our group facilitated Na-ion storage in graphite using solvated-Na-ion intercalation, forming ternary GICs.[15, 16] With the proper selection of the electrolyte, a significant amount of sodium insertion was demonstrated to unexpectedly occur. The Na-ions are stored and reversibly released in graphite for hundreds of cycles assisted by ether-based electrolyte which shows a stability at the potential below 4.0 V (*vs.* Na).[16] Nevertheless, understanding of the mechanism of solvated-Na-ion intercalation in graphite remains limited because of the complexity of the system and the difficulty of quantifying the intercalation of both the solvent molecules and Na ions. The lack of understanding of how and when the Na ion intercalation occurs in graphite prohibits the further advancement of this practically important anode material for Na-ion batteries. Herein, we investigated the intercalation mechanism of Na in graphite by precisely determining the crystal structures and stoichiometry of GICs in the ternary Na-ether-graphite system using *in operando* X-ray diffraction (XRD) analysis coupled with electrochemical titration. The formation of first-stage GICs was directly visualized using real-time measurements of the graphite intercalation. Density functional theory (DFT) calculations suggested a particular configuration of the Na ions and solvent between the graphene layers, which involves the double stacking of solvated-Na-ions. Furthermore, by introducing various solvents, we propose a feasible strategy to tune the energy storage capability of solvated-ion-intercalation-based electrodes.

Results and discussion

Staging behavior upon Na intercalation

To probe the structural evolution of graphite during the intercalation/deintercalation, we obtained synchrotron-based XRD patterns of the electrode *in operando* (5A XRD beamline at PLS-II). For the analysis, a coin-type Na half-cell with a pin-hole containing an ~40-μm thick graphite electrode and ~100 μl of a 1 M $NaPF_6$ in diethylene glycol dimethyl ether (DEGDME) electrolyte was discharged and charged under a current density of 20 mA $g^{-1}_{graphite}$. Each diffraction pattern was collected within a time corresponding to the capacity of ~0.87 mAh $g^{-1}_{graphite}$ (~2.6 min), which enabled the detection of the structural transformation even with the minutest alteration of Na contents. Throughout the electrochemical sodiation and desodiation, the pristine graphite transformed into multiple new phases involving one- or two-phase reactions and was completely restored to the pristine state after a cycle (Fig. 1). The highly reversible structural transformation implies the stable capacity retention of the graphite electrode, which will be further discussed later.

Surprisingly, the evolution of the XRD patterns of the graphite electrode in Fig. 1 indicates a typical staging behavior during electrochemical sodium insertion and extraction even though co-intercalation was expected. The main (002) peak at 27° splits into two peaks, which can be indexed as (*00l*) and (*00l+1*).[17] Applying Bragg's law, we determined the *l*-value using equations 1 and 2, which resulted in equation 3.

$$d_{(00l)} = \frac{I_c}{l} \text{ and } d_{(00l+1)} = \frac{I_c}{l+1} \quad (1)$$

$$d_{(00l)} \sin\theta_{(00l)} = d_{(00l+1)} \sin\theta_{(00l+1)} \quad (2)$$

$$l = \frac{1}{\left[\frac{\sin\theta_{00l+1}}{\sin\theta_{00l}} - 1\right]} \quad (3)$$

, where $d_{(00l)}$ and $d_{(00l+1)}$ are the d-spacing values of the *(00l)* and *(00l+1)* planes, respectively. I_c is the *c* lattice parameter of each stage GIC corresponding to the repeated distance.

During the initial period of sodiation, the graphite undergoes a one-phase-like transformation, possibly with many different stages changing sensitively with a small alteration of the Na

 This journal is © The Royal Society of Chemistry 20xx

Please do not adjust margins

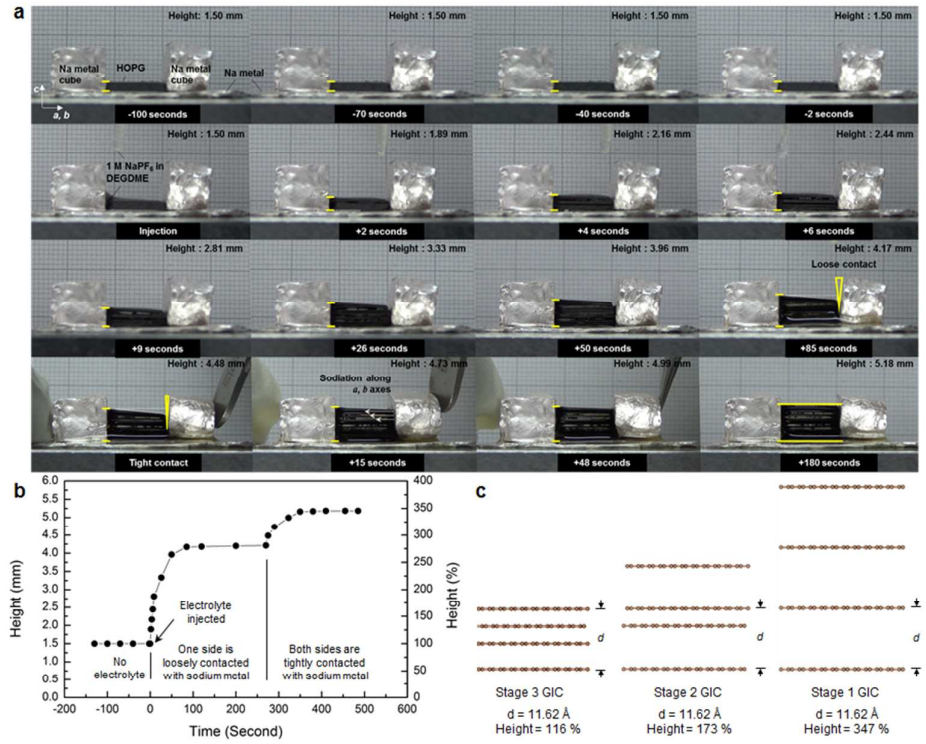

Figure 2. Expansion of highly ordered pyrolytic graphite (HOPG) along the *c* axis with chemical Na-ether intercalation. a. Real-time snapshots of HOPG under direct contact with Na metal before and after exposure to 1 M $NaPF_6$ in DEGDME solution, **b.** height of HOPG measured during the intercalation process, and **c.** schematic comparison of the height and *c* lattice parameter of graphite for hypothetical stage 3 GIC, 2 GIC, and stage 1 GIC.

content. The transformation continues until the specific capacity of graphite reaches 31 mAh $g^{-1}_{graphite}$ (Na: C = 1/72 or 1.5 hour), forming a certain stage of *n* GIC, where the *n* value will be determined later. The measurements of θ_{00l} and θ_{00l+1} at this state suggest *l* = 5 according to equation 3; thus, the two peaks are indexed as (005) and (006), respectively. The determination of *l* also results in I_c from equation 1 above, which is plotted as a function of charge and discharge in the middle of Fig. 1. Between 1.5 and 2.2 h of sodiation (Na: C = 1/50), a biphasic reaction begins to occur, as indicated in the inset box of Fig. 1 left, forming another phase of a stage *o* GIC at the expense of stage *n* GIC. After the completion of the biphasic reaction into stage *o* GIC, a stage *p* GIC evolves. A single phase of stage *p* GIC is observed after 4 h of sodiation, corresponding to a wide range of Na/C from 1/28 to 1/21 with no significant change in the XRD patterns. During the final step of sodiation, as the state of discharge exceeds 91%, new peaks at 12–14° begin to appear. Although further study is required for clarification, we expect that these new peaks originate from the in-plane superstructural ordering of the Na ions and ether solvent molecules, which will be discussed in detail later. Note that the *c* lattice parameters (I_c) of the stage *n*, *o*, and *p* GICs correspond to 18.50, 15.06, and 11.62 Å, respectively. The differences between the I_c values are approximately 3.44 Å, which is similar to the interlayer distance of the pristine graphite (3.35 Å). This finding indicates that the stage numbers *n*, *o*, and *p* are consecutive integers of *p*+2, *p*+1, and *p*, respectively. Considering that I_c of stage *p* (11.62 Å) is less than four times the interlayer distance of pristine graphite (3.35 Å× 4 =13.4 Å), *p* should be less than 4.

To determine the final stage index *p*, we employed chip-type highly ordered pyrolytic graphite (HOPG) with 10×10×1.5 mm dimensions (0.8° mosaic spread) and monitored the height of the HOPG perpendicular to the basal plane in real time using a digital camcorder while intercalating Na and DEGDME solvent (Fig. 2a and Supplementary Video). The HOPG chip was placed on the Na-metal foil and between the two Na-metal cubes to make contact with the graphite layers in both the parallel and vertical directions. The intercalation does not occur in the absence of the electrolyte even though the HOPG and Na metal are physically in contact each other (the first row of Fig. 2a and Fig. 2b). This result contrasts with the case of lithium metal, where the physical contact between lithium metal and graphite leads to rapid lithiation even in the absence of the electrolyte and confirms the thermodynamic instability of the sodiated graphite. However, as soon as we inject the electrolyte (row 2, column1 of Fig. 2a), the HOPG of lateral size of 10 mm immediately swells from the interface, indicative of the Na-ether co-intercalation. Note that this visually noticeable intercalation occurs in less than 2 s. In a few minutes (85 seconds), the height of the HOPG converges to 278% of that of the pristine state. A slight imbalance of the height results from the poor contact between the HOPG and Na-metal cube, as indicated by the yellow triangle in Fig. 2a (row 3, column 4). By tightening up the contact along the *a* and *b* directions of HOPG, the expansion further proceeded rapidly. This observation clearly demonstrates that the Na diffusion occurs

Please do not adjust margins

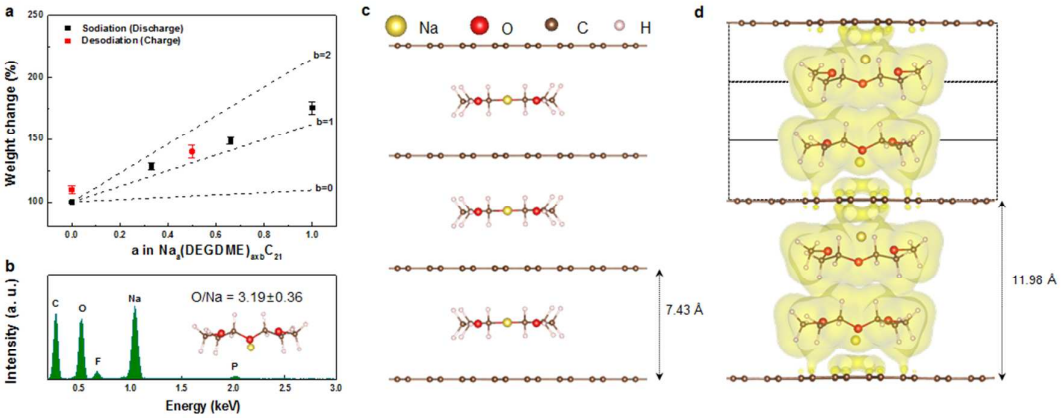

Figure 3. Geometry of solvated-Na intercalated graphite. a. Weight change of graphite measured at various state of charge and discharge. **b.** Energy-dispersive X-ray spectroscopy analysis of discharged sample. Calculated structure when **c.** one [Na-DEGDME]$^+$ complex is and **d.** two [Na-DEGDME]$^+$ complexes are intercalated in the interlayer spacing in graphite.

along the *a* and *b* axes of graphite. In the end, the height of the HOPG was saturated at 346% of that of the pristine state. This value is remarkably close to the theoretically estimated height expansion (347%), assuming the formation of a stage 1 GIC with a *c* lattice parameter of 11.62 Å (Fig. 2c). Similar calculations assuming stage 2 or 3 GICs yielded height expansions of 173% and 116%, respectively, strongly supporting the conclusion that *p* is 1. Thus, *o* and *n* are 2 and 3, respectively.

Solvated-Na-ion intercalation into graphite structure

To better understand the solvated Na intercalation mechanism, we attempted to quantify the number of intercalated DEGDME molecules per Na ion in the graphite by monitoring the weight of the electrode. The weight changes of the graphite electrode were checked at several states of charge and discharge (Fig. 3a). To exclude the weight change from the residual free solvents adsorbed on the electrode surface, the graphite electrodes were dried at 60 °C for 24 h after being disassembled from the coin cells. All the sampling procedures were conducted in an Ar-filled glove box to prevent contamination. The dashed lines in Fig. 3a show the theoretical weight changes of the electrode when different numbers of DEGDME molecules per Na ion (*b*-value) were assumed to be intercalated into the graphite. It is apparent that the weight of the graphite electrode follows the *b*=1 line, which corresponds to a 1:1 ratio of the DEGDME molecules and Na ions in the GICs. The experimental values are slightly higher than the theoretical ones because of the solid-electrolyte-interphase

(SEI) formation upon discharge. This finding is also supported by the energy-dispersive X-ray spectroscopy analysis (Fig. 3b), which indicates that the ratio of O to Na atoms in the GICs is approximately three, confirming that one DEGDME molecule ($(CH_3OCH_2CH_2)_2O$) is intercalated with one Na ion.

We further built model structures to illustrate how the Na ions and DEGDME molecules are co-intercalated in the graphite electrode, given that one Na ion is intercalated into graphite with one DEGDME molecule. Because it is generally believed that the cation and solvent molecules are co-intercalated, maintaining the solvation complex form into graphite,[16, 18-20] the most stable solvation structure of the [Na-DEGDME]$^+$ complex was first determined using first-principles calculations (see Supplementary Fig. 1). The most stable [Na-DEGDME]$^+$ complex is the form where three oxygen atoms of DEGDME are simultaneously coordinating Na ions, as illustrated in Supplementary Fig. 1. Maintaining this initial complex form in the graphite, various configurations of stage 1 GICs were calculated (Supplementary Fig. 2), and three representative models that most sensitively affect the interlayer space of GICs were selected for comparison (Fig. 3c, 3d, and Supplementary Fig. 3). One model consists of a stage 1 GIC with single [Na-DEGDME]$^+$ complex intercalation in the middle of the graphite gallery (Fig. 3c). Another model consists of double stacked [Na-DEGDME]$^+$ complexes located at one-third and two-thirds of the height of the gallery space (Fig. 3d). The final model contains triple stacked [Na-DEGDME]$^+$ complexes in the space (Supplementary Fig. 3). Among all the candidate configurations, the double stacking of the complex was observed to be the most energetically stable model structure, as described in Fig. 3d. When we consider the planar area density of the [Na-DEGDME]$^+$ complex (68.13 Å^2 per complex) within a graphene layer (2.64 Å^2 per carbon atom), the maximum Na concentration in the stage 1 GIC is [Na-DEGDME]$C_{25.8}$, [Na-DEGDME]$C_{12.9}$, and [Na-DEGDME]$C_{8.6}$ for the single, double, and triple stacking models, respectively (see supplementary Fig. 4). Note that the experimental capacity of the graphite electrode was ~110 mAh $g^{-1}_{graphite}$, which corresponds to one [Na-DEGDME]$^+$ complex per 21 carbon atoms, *i.e.,* [Na-DEGDME]C_{21}. This value exceeds the maximum density of the single stacking [Na-DEGDME]$^+$ complex model, confirming that the intercalation geometry of the graphite electrode cannot be the single stack model and is more likely to be the double or triple stack model. To further confirm the structure of Na-DEGDME-graphite GICs, we compared the calculated interlayer distances of the three different models with the experimentally observed value. The three staging models resulted in interlayer distances of 7.43 Å, 11.98 Å, and 16.40 Å, respectively. Considering that the *c* lattice parameter of the stage 1 GIC is 11.62 Å, as measured by XRD analysis (see

This journal is © The Royal Society of Chemistry 20xx

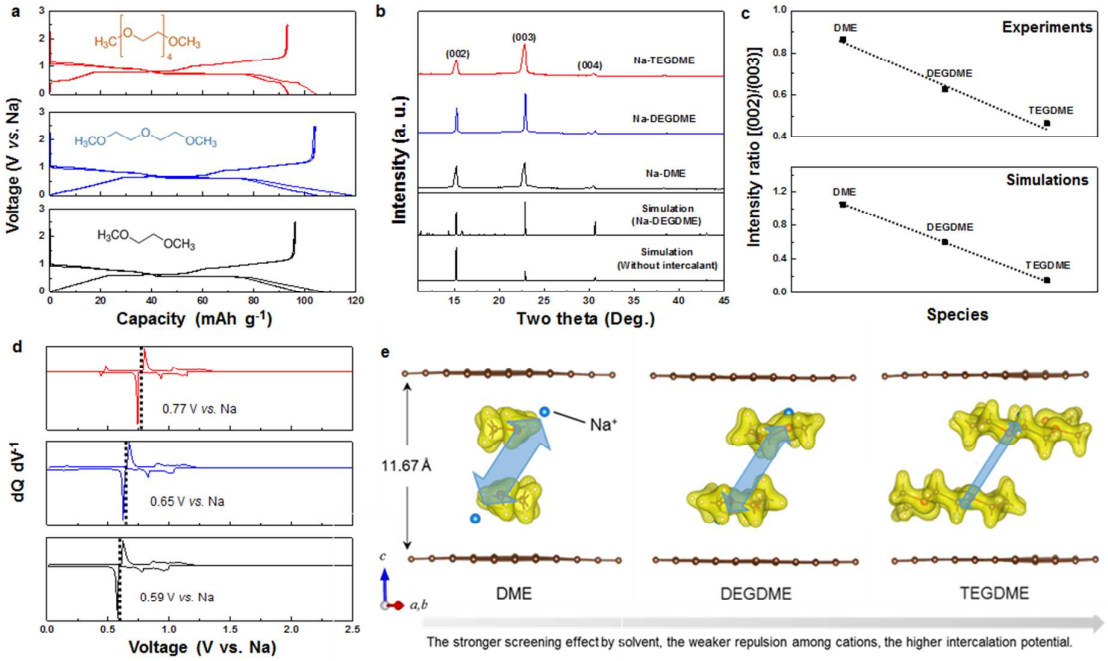

Fig. 1), the second model with double stacking of the complex is much more acceptable with only 3.1 % of a difference (Fig. 3d) compared with the other models.

We further examined the charge interaction between the intercalated $[Na\text{-}DEGDME]^+$ complex and graphene layers. The yellow region in Fig. 3d shows the charge gained after $[Na\text{-}DEGDME]^+$ intercalation (isosurface of 0.017 $e^-/Å^3$). A major portion of the electron cloud, which belongs to the solvent molecules, resides in approximately one-third and two-thirds of the unit cell height because of the electron transfer from the solvating Na ions. Some portion of electrons from the Na ions also moves toward the graphene layers, forming ionic bonds with electrons donated from C-C bonds in the graphene layers (see supplementary Fig. 5), which was similarly observed in Li intercalated graphite.[21]

Solvent dependency of Na intercalation

To understand the correlation between the Na solvation and intercalation, we conducted electrochemical measurements using three different linear ether solvent species with varying chain lengths (*i.e.,* DME, DEGDME, and TEGDME) in Fig. 4. (DME/Na and TEGDME/Na ratios) was observed to be close to unity, which is analogous to the Na-DEGDME electrolyte system (see Supplementary Fig. 6). The *ex situ* XRD analyses of each electrode also revealed similar staging behavior with intercalation, as observed in Supplementary Fig. 7, 8, and 9.

Even the XRD patterns of the fully discharged samples in Na-TEGDME, Na-DEGDME, and Na-DME systems were almost identical, exhibiting sharp (002) and (003) peaks at 15.2° and 22.9° with the same *c* lattice parameters of 11.62 Å (Fig. 4b). This finding implies that the chains of each solvent in $[Na\text{-}ether]^+$ complexes do not stretch along the c direction and thus do not affect the spacing of graphene layers, in accordance with the complex model suggested above. The observed XRD patterns match well with the simulated ones from the double stacking model in Fig. 3d with $[Na\text{-}ether]^+$ complexes residing parallel to the graphene layers at one-third and two-thirds of the height of the gallery. We observed that the ordering of $[Na\text{-}DEGDME]^+$ complexes in the model structure result in minor peaks in the 11˚–22˚ region in the simulated XRD patterns. These peaks rise and diminish as the degree of ordering is artificially modified (see Supplementary Fig. 10). This finding supports the presence of the in-plane superstructural ordering of $[Na\text{-}DEGDME]^+$ complexes at highly discharged graphite electrodes and is consistent with the experimental result in Fig. 1. Note that in Fig. 4b, the (002)/(003) peak ratios differ among the Na-DME, Na-DEGDME, Na-TEGDME systems. The relative intensity of the (003) peak linearly increases with the length of the solvent, as observed in Fig. 4c for both simulations and experiments. As the peak intensity of the (003) plane is determined by the

Figure 4. Na storage potential depending on solvent species. a. Typical charge/discharge profiles of graphite electrode with three electrolyte solvents (inset: solvent molecules) in Na half-cell configuration. **b.** X-ray diffraction (XRD) patterns of solvated-Na intercalated graphite compounds and simulated XRD patterns of expanded graphite with repeated distance of 11.66 Å with/without intercalants of $[Na\text{-}DEGDME]^+$ complex. **c.** Intensity ratio of (002)/(003) when three electrolyte solvents are intercalated into graphite with Na ions. **d.** dQ dV^{-1} analysis of graphite electrode with three electrolyte solvents. **e.** Schematic of the screening effect of the solvent on the Na storage potential.

Notably, the specific capacity and shape of the charge/discharge profiles were not greatly affected by the solvent species despite their different molecular sizes and weights. The coordination number of complexes in each case

Please do not adjust margins

electron density in the plane, the higher electron density offered by the solvent with the longer chain, *i.e.,* Na-TEGDME, results in the smallest (002)/(003) peak intensity ratio in Fig. 4c.

Note that the Na storage potential increases as the chain length of the solvent species increases. Voltage plateaus were observed at 0.59, 0.65, and 0.77 V (*vs.* Na) in DME, DEGDME, and TEGDME, respectively (Fig. 4d). This correlation provides strong evidence for solvated-Na-ion intercalation. The solvent-dependent Na storage voltage is attributable to the screening effect by the solvent molecules. Generally, the Na storage voltage is described by the energy difference between pristine (here, graphite) and intercalated products (here, the Na-solvent-graphite compound). In our case, the energetics of the intercalated products primarily determines the difference in the overall Na storage voltage, given the same pristine material. Because neutral molecules in the graphite galleries can stabilize the intercalated product by screening the repulsion between positively charged Na ions,[22] a stronger screening effect is expected with longer chain solvent species, which in turn will increase the Na storage potential (Fig. 4e).

It remains unclear why these unique phenomena are observed only in electrochemical systems using specific solvents (*i.e.,* DME, DEGDME, and TEGDME). This solvent dependency of solvated-ion intercalation phenomenon is also reported in Li-graphite systems,[23-25] where various behaviors such as binary, ternary intercalation and exfoliation of graphite are observed depending on the solvent species. Although further study is needed, a possible interpretation is that the linear ether solvents strongly solvate Na ions primarily because of the enhanced affinity between the solvent and Na ions resulting from the so-called chelate effect.[26, 27] Considering Na ion solvation with two distinctive groups of oxygen-containing solvents, (i) solvents with a linear chain such as the linear ethers used in this work and (ii) solvents without a linear chain such as cyclic ethers or carbonates, multiple oxygen atoms in one solvent molecule can more efficiently surround the Na ion if group (i) solvents are used due to the geometric flexibility. This behavior will stabilize the solvation structure, as calculated in this work. To achieve a similar solvation enthalpy (*i.e.,* to provide the same donor power with solvent molecules) with group (ii) solvents, more than one solvent molecule is required to form a similar Na-O local environment because of their geometric limitation. In these two cases, the enthalpy of solvation is approximately the same because similar donor power is provided. However, there is a major difference in the two reactions, that is, the number of species participating in each reaction. Solvation with group (i) solvents involves two species (one solvent molecule and one Na ion) to form one solvation complex; however, more than two species (more than one solvent molecules and one Na ion) should participate in the latter to provide a similar Na-O local environment. Therefore, if we compare the loss of the entropy of disorder in the two cases, less entropy of disorder is lost in solvation with group (i) solvents, resulting in more favorable solvation.

It is worthy of noting that a remarkably high reversibility in the co-intercalation is possible for the Na-ether-graphite system even with the exceptionally large volume change of the electrode. It is generally known that the volume change greatly affects the cycle performance of the electrode for rechargeable batteries.[28] The large volume change of the electrode gradually degrades the structure of the electrode, leading to severe performance decay. For example, the poor cycle stability of a few important electrode materials, such as Si and SnO_2, is attributed to their large volumetric change.[29, 30] Although the graphite electrode undergoes an exceedingly large volume change of 347% upon charge/discharge, it exhibits excellent cycle stability up to 2,500 cycles (see Ref. 16 and Supplementary Fig. 11 and Fig. 12). Note that no noticeable structure degradation in either the bulk or surface of the graphite electrode was observed after cycling in the Na-DEGDME electrolyte system (Supplementary Fig. 13 and Fig. 14). We attribute the excellent reversibility to (i) the formation of ionic binding between Na and the graphene layer, as observed in Supplementary Fig. 5 despite the large expansion of the gallery space preventing the exfoliation of graphene layers, and (ii) the much more stable solvation complex in the graphite gallery compared with the propylene-carbonate-based solvation complex, wherein intercalated propylene carbonate solvents are decomposed into gas phases and readily exfoliate graphene layers.[31-33] For more practical applications of ternary GIC systems, it also needs to investigate Na-containing electrolytes with better oxidative stability (>4.0 V *vs.* Na).

There have also been some reports on the electrochemical storage of cations in host materials, which can be switched on with the aid of proper solvents similar to our system, indicative of the importance of the role of electrolyte solvents.[16, 34, 35] In this respect, our work enriches the pool of electrode materials, which has been limited to the binary systems of guest ion-host materials, to versatile ternary systems of guest ion-solvent-host materials. These findings will lead us to further investigations toward energy-storage materials using solvated-ion intercalation.

Conclusions

We investigated the solvated-ion intercalation chemistry of the ternary GIC system of Na-ether-graphite, which has been poorly understood because of its complexity compared with the simple binary GIC system of Li-graphite. *In operando* XRD-electrochemical analysis and direct visualization coupled with DFT calculations revealed the structural evolution of the graphite during the solvated-Na intercalation. The Na intercalation occurs through multiple staging reactions, which finally form first-stage GICs within a wide range of Na/C from 1/28 to 1/21 with excellent reversibility. We proposed that the intercalated Na ions and ether solvents are in the form of $[Na\text{-}ether]^+$ complexes double stacked in parallel with graphene layers in the graphite galleries. The correlation between the solvent species and intercalation suggests the possible tunability of Na storage properties. The Na storage potential increases as the chain length of the solvent species increases because of the stronger screening effects of longer solvent

 This journal is © The Royal Society of Chemistry 20xx

Please do not adjust margins

molecules on the repulsion between positively charged Na ions in the discharge product. This work suggests that various unexplored ternary intercalation systems of guest ion-solvent-host materials can provide unlimited opportunities to design electrodes with superior performances beyond that of conventional electrode materials of rechargeable batteries.

Acknowledgements

This work was supported by (i) the Human Resources Development program (20124010203320) of the Korea Institute of Energy Technology Evaluation and Planning (KETEP) grant funded by the Korea government Ministry of Trade, Industry and Energy. (ii) the Energy Efficiency & Resources of the Korea Institute of Energy Technology Evaluation and Planning (KETEP) grant funded by the Korea government Ministry of Trade, Industry & Energy (MOTIE) (No.20132020000270).

Notes and references

1. L. B. Ebert, *Annu. Rev. Mater. Sci.*, 1976, **6**, 181-211.
2. M. S. Dresselhaus and G. Dresselhaus, *Adv. Phys.*, 1981, **30**, 139-326.
3. T. E. Weller, M. Ellerby, S. S. Saxena, R. P. Smith and N. T. Skipper, *Nat. Phys.*, 2005, **1**, 39-41.
4. K. Sugihara, *Phys. Rev. B*, 1988, **37**, 4752-4759.
5. K. Sugihara, *Phys. Rev. B*, 1984, **29**, 5872-5877.
6. H. Cheng, X. Sha, L. Chen, A. C. Cooper, M.-L. Foo, G. C. Lau, W. H. Bailey Iii and G. P. Pez, *J. Am. Chem. Soc.*, 2009, **131**, 17732-17733.
7. A. Grüneis, C. Attaccalite, A. Rubio, D. V. Vyalikh, S. L. Molodtsov, J. Fink, R. Follath, W. Eberhardt, B. Büchner and T. Pichler, *Phys. Rev. B*, 2009, **80**, 075431.
8. K. Kanetani, K. Sugawara, T. Sato, R. Shimizu, K. Iwaya, T. Hitosugi and T. Takahashi, *Proc. Nat. Acd. Sci.*, 2012, **109**, 19610-19613.
9. M. Conti-Ramsden, K. Nkrumah-Amoako, N. Brown and E. L. Roberts, *Adsorption*, 2013, **19**, 989-996.
10. S. Park and R. S. Ruoff, *Nat. Nanotechnol.*, 2009, **4**, 217-224.
11. Y. Nishi, *J. Power Sources*, 2001, **100**, 101-106.
12. D. Aurbach and Y. Ein-Eli, *J. Electrochem. Soc.*, 1995, **142**, 1746-1752.
13. K. Nobuhara, H. Nakayama, M. Nose, S. Nakanishi and H. Iba, *J. Power Sources*, 2013, **243**, 585-587.
14. Z. Wang, S. M. Selbach and T. Grande, *RSC Adv.*, 2014, **4**, 4069-4079.
15. B. Jache and P. Adelhelm, *Angew. Chem. Int. Ed.*, 2014, **53**, 10169-10173.
16. H. Kim, J. Hong, Y.-U. Park, J. Kim, I. Hwang and K. Kang, *Adv. Funct. Mater.*, 2015, **25**, 534-541.
17. J. A. Seel and J. R. Dahn, *J. Electrochem. Soc.*, 2000, **147**, 892-898.
18. W. Sirisaksoontorn, A. A. Adenuga, V. T. Remcho and M. M. Lerner, *J. Am. Chem. Soc.*, 2011, **133**, 12436-12438.
19. Y. Yamada, K. Usui, C. H. Chiang, K. Kikuchi, K. Furukawa and A. Yamada, *ACS Appl. Mater. Interf.*, 2014, **6**, 10892-10899.
20. H. Moon, R. Tatara, T. Mandai, K. Ueno, K. Yoshida, N. Tachikawa, T. Yasuda, K. Dokko and M. Watanabe, *J. Phys. Chem. C*, 2014, **118**, 20246-20256.
21. G. Yoon, D.-H. Seo, K. Ku, J. Kim, S. Jeon and K. Kang, *Chem. Mater.*, 2015, **27**, 2067-2073.
22. N. I. Kovtyukhova, Y. Wang, A. Berkdemir, R. Cruz-Silva, M. Terrones, V. H. Crespi and T. E. Mallouk, *Nat. Chem.*, 2014, **6**, 957-963.
23. Y. Mizutani, T. Abe, M. Inaba and Z. Ogumi, *Synthetic Met.*, 2001, **125**, 153-159.
24. Y. Yamada, Y. Takazawa, K. Miyazaki and T. Abe, *J. Phys. Chem. C*, 2010, **114**, 11680-11685.
25. T. Abe, N. Kawabata, Y. Mizutani, M. Inaba and Z. Ogumi, *J. Electrochem. Soc.*, 2003, **150**, A257-A261.
26. G. Schwarzenbach, *Helv. Chim. Acta*, 1952, **35**, 2344-2359.
27. R. D. Hancock and A. E. Martell, *Comment Inorg. Chem.*, 1988, **6**, 237-284.
28. Y.-U. Park, D.-H. Seo, H.-S. Kwon, B. Kim, J. Kim, H. Kim, I. Kim, H.-I. Yoo and K. Kang, *J. Am. Chem. Soc.*, 2013, **135**, 13870-13878.
29. C. K. Chan, H. Peng, G. Liu, K. McIlwrath, X. F. Zhang, R. A. Huggins and Y. Cui, *Nat. Nanotechnol.*, 2008, **3**, 31-35.
30. H. Kim, S.-W. Kim, Y.-U. Park, H. Gwon, D.-H. Seo, Y. Kim and K. Kang, *Nano Res.*, 2010, **3**, 813-821.
31. H. Buqa, A. Würsig, D. Goers, L. J. Hardwick, M. Holzapfel, P. Novák, F. Krumeich and M. E. Spahr, *J. Power Sources*, 2005, **146**, 134-141.
32. M. R. Wagner, J. H. Albering, K. C. Moeller, J. O. Besenhard and M. Winter, *Electrochem. Commun.*, 2005, **7**, 947-952.
33. A. N. Dey and B. P. Sullivan, *J. Electrochem. Soc.*, 1970, **117**, 222-224.
34. H. Pan, X. Lu, X. Yu, Y.-S. Hu, H. Li, X.-Q. Yang and L. Chen, *Adv. Energy Mater.*, 2013, **3**, 1186-1194.
35. Z. Hu, Z. Zhu, F. Cheng, K. Zhang, J. Wang, C. Chen and J. Chen, *Energy Environ. Sci.*, 2015, **8**, 1309-1316.